Current Control of the Coupled-Inductor Buck–Boost DC–DC Switching Converter using a Model Predictive Control Approach

Carlos Restrepo*, Germain Garcia, Freddy Flores-Bahamonde, Duberney Murillo-Yarce, *Student Member, IEEE*, Johan I. Guzman, *Member, IEEE*, and Marco Rivera, *Senior Member, IEEE*.

***Abstract*—Coupled-inductor buck-boost dc-dc switching converter has emerged as an alternative to manage power in several hybrid system architectures. This is due to features such as a noninverting voltage step up and step down characteristic, high efficiency, wide-bandwidth, and the possibility to regulate its input or output currents as has been reported in previous works. All of them are based on a small-signal linearized model around an operating point. In this paper, a model predictive control strategy is proposed in order to increase the operation point domain. The proposal consists in the use of the mathematical model of the system in discrete time to obtain the optimal switching state to be applied in the converter, based on a cost function optimization which simultaneously improves the current tracking and reduces the converter power losses. Experimental results validate the proposal demonstrating that this is a good alternative for the control of this kind of power converters.**

***Index Terms*—Model predictive control, digital control, noninverting buck–boost converter, current control.**

I. Introduction

During the last years, control techniques in power electronic applications have been evolving in order to meet with most demanding control goals due to the increased development of more flexible and distributed power systems [1]. In the same way, recent advances in digital processing systems through the development of more powerful processors, has also allowed the use of complex algorithms enabling the deployment of sophisticated, accurate and robust control techniques, such as non-linear techniques like fuzzy, adaptive, sliding mode and predictive controls [1]–[9].

This work was supported by the Chilean Government under Project CONICYT/FONDECYT 1191680 and the CONICYT-PFECHA/Doctorado Nacional/2019-21191663. The work was also supported by SERC Chile (CONICYT/FONDAP/15110019).

C. Restrepo and M. Rivera are with the Department of Electromechanics and Energy Conversion, Universidad de Talca, Curicó, 3340000, Chile (e-mail: crestrepo@utalca.cl, marcoriv@utalca.cl).

G. Garcia is with LAAS-CNRS, 7 Avenue du colonel Roche, 31077 Toulouse Cedex 4, and INSA, 135, Avenue de Rangueil, 31077 Toulouse Cedex 4, France (e-mail: garcia@laas.fr)

F. Flores-Bahamonde is with the Department of Engineering Sciences, Universidad Andres Bello, Santiago, Chile (e-mail: freddy.flores@unab.cl)

D. Murillo-Yarce is with the Doctorate in Engineering Systems, Faculty of Engineering, Universidad de Talca, Curicó, 3340000, Chile (e-mail: duberney.murillo@utalca.cl).

J. I. Guzman is with the Department of Electrical and Electronic Engineering, Universidad del Bío-Bío, Concepción, Chile (e-mail: joguzman@ubiobio.cl.

*Corresponding author. Email: crestrepo@utalca.cl. Postal Address: Camino Los Niches Km Uno, Curicó, Chile. Telephone number: (+56) 752201815.

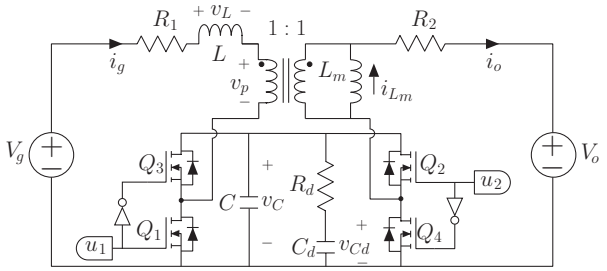

Fig. 1. Schematic circuit diagram of the versatile buck–boost converter.

In order to fulfill with new control requirements flexible and robustness non-linear strategies are commonly used to improve the performance of power converters. One of the most exploited is model predictive control (MPC), and more specifically the finite control set (FCS) MPC which is widely used in power converters for low, medium and high power applications [10]. The fast growth of FCS-MPC is due to its discrete nature, flexibility and capacity to include the constraints and non-linearities of the power system [1], [11]–[15]. Accordingly to its name, by means of the prediction of the future behavior of the system, the main objective of MPC is to select the most appropriate control action based on the optimization of a cost function [9], [10], [16]. The resulting control action is applied selecting one of the switches states defined by the system.

So far, FCS-MPC has been commonly applied to three-phase inverters [17]–[19], but although in less cases, its use in dc–dc converters has been also explored [20]–[23]. In dc–dc applications the use of non-linear techniques is driven by the need to add robustness to the system against high disturbances. Besides, solves stability issues minimizing the effect of high non-linearities and non-minimum phase phenomena existing in some step–up topologies [20], [23]–[25]. This is particularly the case of the coupled–inductor buck–boost converter known as versatile buck–boost converter [26] illustrated in Fig. 1. The main advantage of this power converter is the great versatility allowing its use in different places of hybrid power systems [27]–[29] such as the serial hybrid (SH) topology, the parallel hybrid (PH) topology and the series–parallel hybrid (SPH) topology shown in Fig. 2. In general, its main features can be listed as noninverting voltage step–up and step–down characteristic, high efficiency, wide bandwidth [26], regulation

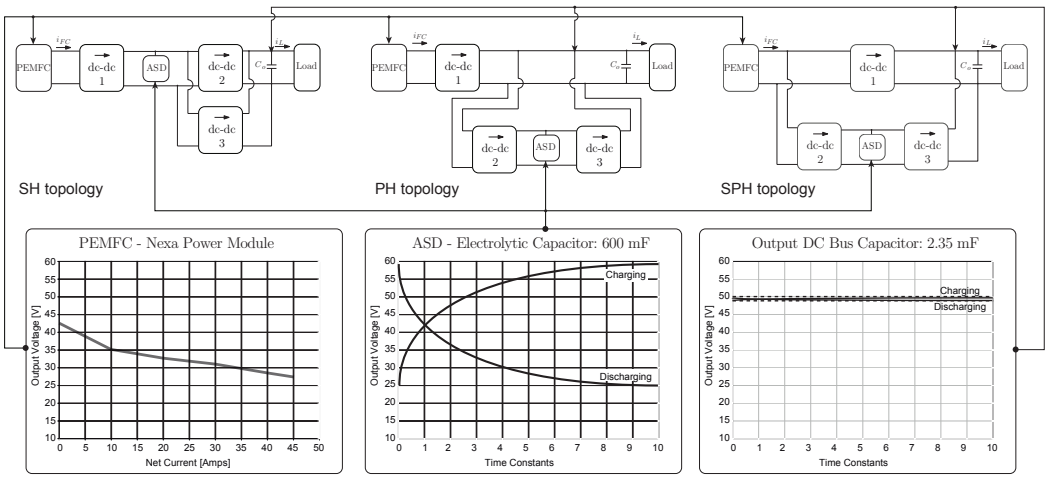

Fig. 2. Hybrid power systems based on the versatile buck–boost converter and its voltage operation range in each terminal.

of input or output currents because of their low ripple values [30], and the ability to change from input to output current regulation loop for suddenly or smoothly demanded changes [31].

Nevertheless, until now the controls developed for this converter have been based on analog and digital PWM linear controls. Consequently, a specific control design is needed for each converter for the corresponding operating point depending on where is located in the system of Fig. 2. Besides, linear control techniques hinder the practical implementation of control loops that prevent specific constraints, such as dead–zones presented in buck-boost converters which may cause instability problems [32].

The main contributions of this paper are:

- The proposal of a model predictive control strategy for the versatile buck–boost converter. This control is an alternative to the well known linear controllers which must operate close to an operating point where the linearization was made.
- A high efficiency operation is reached due to the fact that the converter shown in Fig. 1 only operates in boost mode when ($V_g < V_o$) or buck mode when ($V_g \geq V_o$). This allows not only the reduction of the switching losses but also the reduction of the possible switching states which represents a smaller amount of calculations which are very important to operate at high frequencies.
- With the proposed control a start-up algorithm and a transition technique between the operation modes (boost or buck) are not required.
- The proposed control strategy can be used by all the converters of a hybrid power system which represents a great simplicity of the whole system.

This paper is organized as follows: in Section II the equilibrium states of the dc-dc coupled inductors buck–boost converter is calculated. Section III presents a detailed description of the most relevant aspects of the proposed control technique. Simulations and experimental results of both control techniques are presented and discussed in Section IV. Finally, the main conclusions and the remaining challenges for the future are summarized in Section V.

II. DC-DC Operation Mode

A general analysis of the coupled inductors buck–boost converter shown in Fig. 1 is presented in the Appendix. The retained model of the converter is recalled here

$$\frac{dx(t)}{dt} = A_0 x(t) + B_0(x(t), v(t))\lambda(t) \tag{1}$$

with $\lambda : \mathbb{R} \to \Lambda_S$.

We can relax the control taking $\lambda : \mathbb{R} \to \Lambda_R$ and then the obtained relaxed model is intimately related to the model presented in the Appendix. For the case of a DC-DC operation mode, the voltages V_g and V_0 are supposed constant and $v(t) = V = [V_g, V_0]$. Then, x_e is an equilibrium of the relaxed model if there exits $\lambda_e \in \Lambda_R$ such that

$$A_0 x_e + B_0(x_e, V)\lambda_e = 0 \tag{2}$$

Then

$$x_e = -(A_0 + \lambda_{e_1} A_1 + \lambda_{e_2} A_2 + \lambda_{e_3} A_3 + \lambda_{e_4} A_4)^{-1} BV, \quad \lambda_e \in \Lambda_R \tag{3}$$

After some calculations and using the fact that $\lambda_e \in \Lambda_R$, the set of equilibria ($X_{eq} = x_e : \lambda_e \in \Lambda_R$) of the relaxed model is defined as

$$X_{eq} = \begin{bmatrix} -(\lambda_{e_2} + \lambda_{e_4}) \dfrac{(\lambda_{e_1} + \lambda_{e_2}) V_0 - (\lambda_{e_2} + \lambda_{e_4}) V_g}{R_1 (\lambda_{e_2} + \lambda_{e_4})^2 + R_2 (\lambda_{e_1} + \lambda_{e_2})^2} \\ -(\lambda_{e_1} + \lambda_{e_2}) \dfrac{(\lambda_{e_1} + \lambda_{e_2}) V_0 - (\lambda_{e_2} + \lambda_{e_4}) V_g}{R_1 (\lambda_{e_2} + \lambda_{e_4})^2 + R_2 (\lambda_{e_1} + \lambda_{e_2})^2} \\ \dfrac{R_1 (\lambda_{e_2} + \lambda_{e_4}) V_0 + R_2 (\lambda_{e_1} + \lambda_{e_2}) V_g}{R_1 (\lambda_{e_2} + \lambda_{e_4})^2 + R_2 (\lambda_{e_1} + \lambda_{e_2})^2} \\ \dfrac{R_1 (\lambda_{e_2} + \lambda_{e_4}) V_0 + R_2 (\lambda_{e_1} + \lambda_{e_2}) V_g}{R_1 (\lambda_{e_2} + \lambda_{e_4})^2 + R_2 (\lambda_{e_1} + \lambda_{e_2})^2} \end{bmatrix} \tag{4}$$

The two voltages V_g and V_0 are fixed, but they do not define the buck or boost nature of the conversion operated by the circuit. The buck or boost nature is completely determined by the sense of the currents. For example, if $0 < V_g < V_0$ and if the current are positive, the circuit is a boost. But if the current

are negative, the circuits is a buck. For the first case, the power flows from V_g to V_0 and for the second one, from V_0 to V_g. The converter is bi-directional and offers a great flexibility. We can also note that V_0 and V_g can be simultaneously negative. The mode of operation could be determined depending on the context. Note that at equilibrium, a key parameter is the ratio between currents i_0 and i_g denoted i_{0_e} and i_{g_e}, namely

$$\frac{i_{0_e}}{i_{g_e}} = \frac{\lambda_{e_1} + \lambda_{e_2}}{\lambda_{e_2} + \lambda_{e_4}} = \frac{1}{n_I} \geq 0 \tag{5}$$

Note also that at equilibrium, the voltages v_C and v_{C_d} are such that $v_{C_e} = v_{C_{d_e}}$ and the power balance equation becomes

$$-R_1 i_{g_e}^2 - R_2 {i_{0_e}}^2 + V_g i_{g_e} - V_0 i_{0_e} = 0 \tag{6}$$

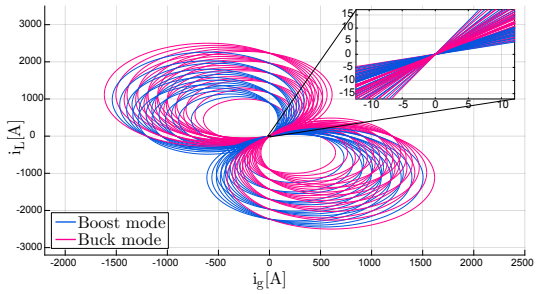

Fig. 3. Currents equilibrium of (7).

After simple calculations, we can verify that each $x_e \in X_{eq}$ is a solution of the previous equation which can also be written as

$$\frac{\left(i_{g_e} - \frac{V_g}{2R_1}\right)^2}{\left(\frac{V_g}{2R_1}\sqrt{1 + \frac{R_1}{R_2} n_V^2}\right)^2} + \frac{\left(i_{0_e} + \frac{V_0}{2R_2}\right)^2}{\left(\frac{V_0}{2R_2}\sqrt{1 + \frac{R_2}{R_1}\frac{1}{n_V^2}}\right)^2} = 1, \quad n_V = \frac{V_0}{V_g} \tag{7}$$

n_V being positive, currents are positive or negative, and the currents equilibrium belong to a portion of an ellipse shown in Fig. 3.

It is also possible to deduce the relation between n_I and n_V. We have

$$\frac{n_V}{n_I} = 1 - \frac{i_{g_e}}{V_g}\left(R_1 + \frac{R_2}{n_I^2}\right) = \frac{1}{1 + (R_2 + n_I^2 R_1)\frac{i_{0_e}}{V_0}} \tag{8}$$

We recover the fact that when $R_1 = R_2 = 0$, the converter is *POPI* (Power Output equal to Power Input) with $n_V = n_I$. Analyzing the circuit behavior and the expression of v_{C_e} and $v_{C_{d_e}}$, we can also deduce that $v_{C_e} = v_{C_{d_e}} \leq \max\{V_g, V_0\}$. Indeed, we have

$$\begin{aligned} v_{C_e} = \quad & v_{C_{d_e}} = \frac{R_1(\lambda_{e_2} + \lambda_{e_4})V_0 + R_2(\lambda_{e_1} + \lambda_{e_2})V_g}{R_1(\lambda_{e_2} + \lambda_{e_4})^2 + R_2(\lambda_{e_1} + \lambda_{e_2})^2} \\ & v_{C_{d_e}} \leq \frac{R_1(\lambda_{e_2} + \lambda_{e_4})^2 V_0 + R_2(\lambda_{e_1} + \lambda_{e_2})^2 V_g}{R_1(\lambda_{e_2} + \lambda_{e_4})^2 + R_2(\lambda_{e_1} + \lambda_{e_2})^2} \end{aligned} \tag{9}$$

$$\begin{aligned} v_{C_e} = \quad & \frac{\left[R_1(\lambda_{e_2} + \lambda_{e_4})^2 n_V + R_2(\lambda_{e_1} + \lambda_{e_2})^2\right] V_g}{R_1(\lambda_{e_2} + \lambda_{e_4})^2 + R_2(\lambda_{e_1} + \lambda_{e_2})^2} \\ = \quad & \frac{\left[R_1(\lambda_{e_2} + \lambda_{e_4})^2 + \frac{R_2(\lambda_{e_1} + \lambda_{e_2})^2}{n_V}\right] V_0}{R_1(\lambda_{e_2} + \lambda_{e_4})^2 + R_2(\lambda_{e_1} + \lambda_{e_2})^2} \end{aligned} \tag{10}$$

If $n_V > 1$ then $v_{C_e} = v_{C_{d_e}} \leq V_0$ and if $n_V < 1$ then $v_{C_e} = v_{C_{d_e}} \leq V_g$. Note that if V_0 and V_g are negative, a similar analysis leads to $v_{C_e} = v_{C_{d_e}} \geq \min\{V_g, V_0\}$. It is also possible to express the set of equilibrium states in terms of parameters n_I and n_V introduced above. In such a case, $X_{eq} = \{x_e : \lambda_e \in \Lambda_R,\ n_I > 0,\ n_V > 0\}$ and we obtain

$$x_e = \left[\frac{n_I^2(1 - \frac{n_V}{n_I})V_g}{n_I^2 R_1 + R_2}, \frac{n_I(1 - \frac{n_V}{n_I})V_g}{n_I^2 R_1 + R_2}, \frac{(n_I n_V R_1 + R_2)}{(n_I^2 R_1 + R_2)} \cdot \frac{V_g}{(\lambda_{e_1} + \lambda_{e_2})}, \frac{(n_I n_V R_1 + R_2)V_g}{(\lambda_{e_1} + \lambda_{e_2})(n_I^2 R_1 + R_2)}\right]^T$$

We can conclude that the flow of power in the converter is completely determined by the values of n_I, n_V and the signs of V_0 and V_g. To end with analysis of the possible steady-states, remark that in the expressions (4), λ_{e_3} does not appear explicitly. λ_{e_3} is associated with the converter mode corresponding to $u_1 = 1$ and $u_2 = 0$. Because the two last components of equilibrium states are equal, the selection of an equilibrium can be done, only fixing the first third components and selecting appropriately λ_{e_1}, λ_{e_2} and λ_{e_4}. It is possible to impose $\lambda_{e_3} = 0$ meaning that, in steady-state, the control $u_1 = 1$ and $u_2 = 0$ will be discarded. We can remark that in this mode, the capacitors C, C_d and resistor R_d are isolated and some care has to be taken to prevent important variations of inductor currents which could destroy some converter components. In practice, it is better to discard this mode to prevent such problems.

From a practical point of view, the interest of the versatile converter is its possibility to work as a buck or a boost operation modes. Considering V_g as the voltage of the power source and V_0 as the voltage of the power load, these two operation modes are characterized by

i) For the buck mode, $u_1 = 0$ and u_2 commutes
ii) For the boost mode, u_1 commutes and $u_2 = 1$

The resulting control problem consists of stabilizing the converter around a specific steady states characterized by a vector $x_e \in X_{eq}$. We are now in position to state precisely the MPC control strategy.

III. FCS–MPC FOR THE INPUT CURRENT OF THE VERSATILE BUCK–BOOST CONVERTER

A. Proposed control scheme

In this section a detailed description of the FCS–MPC to control the input current i_g is presented. The interest of controlling this variable is because a rectifier design based on the versatile converter is a work in progress.

With the above set of equations and the measurement of the converter state variables (i_g. v_g, v_C, v_{C_d}, i_o and v_o) under a constant sampling frequency T_s, it is possible to predict the future behavior of the controlled variables in the next sampling (one–sample horizon algorithm is considered) for the different values of the control $\lambda((k+1)T_s) = \lambda[k+1]$. Recall that

the combination $u_1 = 1$ and $u_2 = 0$ which corresponds to $\lambda = [0, 0, 1, 0]^T$was discarded and then

$$\lambda[k+1] \in \Lambda_C = \left\{ \begin{bmatrix} 1 \\ 0 \\ 0 \\ 0 \end{bmatrix}, \begin{bmatrix} 0 \\ 1 \\ 0 \\ 0 \end{bmatrix}, \begin{bmatrix} 0 \\ 0 \\ 0 \\ 1 \end{bmatrix} \right\} \tag{11}$$

Each possible value of $\lambda[k+1]$ is associated to a switch configuration (u_1, u_2).

B. Cost function

The objective is to control the input current (i_g) but considering an additional requirement which is the reduction of power losses to ensure an efficient converter performance in all the operation points. A way to attain this objective is to solve at each step, the following optimization problem

$$\min_{\lambda[k+1]\in\Lambda_C} g\left(\lambda\left[k+1\right]\right) \tag{12}$$

where

$$g(\lambda\left[k+1\right]) = K_{i_0}\left(i_{0ref}\left[k+1\right] - i^p_{0_{\lambda[k+1]}}\right)^2 + K_{i_g}\left(i_{gref}\left[k+1\right] - \frac{i^p_{g_{\lambda[k+1]}} + i_g\left[k\right] + i_g\left[k-1\right]}{3}\right)^2 \tag{13}$$

$i_{gref}[k+1]$ is the input current reference by the sampling period $k+1$, $i^p_{g_{\lambda[k+1]}}$ is the prediction of the input current for the instant $[k+1]$ when control $\lambda[k+1]$ is applied, $i_g\left[k\right]$ is the actual current measurement and $i_g\left[k-1\right]$ is the last measure of current. In this cost function for the input current error an average value of three points is used with the aim of achieving an average input current value close to the reference in each sampling. In this cost function, $i^p_{0_{\lambda[k+1]}}$ is the prediction of the output current for the instant $[k+1]$ when control $\lambda[k+1]$ is applied, and $i_{oref}[k+1]$ the output current reference by the sampling period $k+1$ which can be calculated from (6) to reduce the converter power losses in the damping resistor R_d.

$$i_{oref}[k+1] = \frac{v_o[k]}{2R_2}\left[\left(1 + (v_g[k] - R_1\ i_{gref}[k+1])\cdot \frac{4\ R_2\ i_{gref}[k+1]}{v_o^2[k]}\right)^{\frac{1}{2}} - 1\right] \tag{14}$$

K_{i_g} and K_{i_0} are the weighting factors to adjust the currents reference tracking i_{gref} and i_{oref}, respectively. These factors were tuned by means of several simulations of the versatile buck–boost converter under the buck and boost operation modes with the goal of reducing the tracking error of the input and output currents. The selected criteria used to measure the error between the converter currents (i_g and i_0) and their respective references (i_{gref} and i_{oref}) for specific weighting factors (K_{i_g} and K_{i_0}) was the mean absolute percentage error (MAPE), which is defined as

$$\text{MAPE}\ (i_x) = \frac{100\%}{n} \cdot \sum_{t=1}^{n} \left| \frac{i_{refx} - i_x}{i_{refx}} \right|, \tag{15}$$

where $(i_{refx} - i_x)$ is the error between the simulated current (i_x) and its respective reference (i_x), and n is the number of steps of the simulation. For the selection of the weighting factors, a known value for $K_{i_g} = 10$ was assumed. After this, different simulations were performed in both boost and buck modes and its respective MAPE was calculated for each value of K_{i_0} as shown in Fig. 4. The simulation for the selection of the weighting factors includes starting and reference changes of the current. From Fig. 4, it is evident that the minimum MAPE is obtained with a $K_{i_0} = 0.1$.

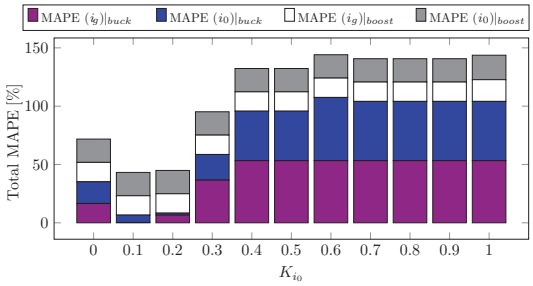

Fig. 4. Total MAPE of current reference tracking for $K_{i_g} = 10$ as function of the K_{i_0}

C. Prediction model

The predicted values for the currents $i^p_{g_{\lambda[k+1]}}$ and $i^p_{0_{\lambda[k+1]}}$ are obtained by discretizing the model (A.11) by Euler method leading to the discrete-time model

$$x[k+1] = (I + T_s \cdot A_0)x[k] + T_s \cdot B_0(x[k], v[k])\ \lambda[k] \tag{16}$$

where I is the identity matrix of appropriate dimensions.

D. Algorithm description

Fig. 5 shows the time diagram of the execution of the FCS–MPC algorithm proposed by the versatile buck–boost converter. The FCS-MPC algorithm has the following basic steps:

- Measure the converter signals ($i_g[k]$. $v_g[k]$, $v_C[k]$, $v_{Cd}[k]$, $i_o[k]$ and $v_o[k]$) and the desired reference value ($i_{ref}[k+1]$) in the sampling period $k+1$.
- Apply the optimal switching state $\lambda_{opt}[k]$ which was computed in the previous sampling period $(k-1)T_s$.
- For each $\lambda[k+1] \in \Lambda_C$, the mathematical model allows to predict the behavior of the converter's variable in the next sampling interval ($i^p_{g_{\lambda[k+1]}}$, $v^p_{C_{\lambda[k+1]}}$, $v^p_{C_{d_{\lambda[k+1]}}}$, and $i^p_{o_{\lambda[k+1]}}$) using model (16).
- Evaluate the cost function $g(\lambda[k+1])$ for each $\lambda[k+1] \in \Lambda_C$.
- Select the control $\lambda[k+1]$ that minimizes the cost function $g(\lambda[k+1])$.
- Store $\lambda_{opt}[k+1]$ which will be applied to the converter in the next sampling period $k+1$.

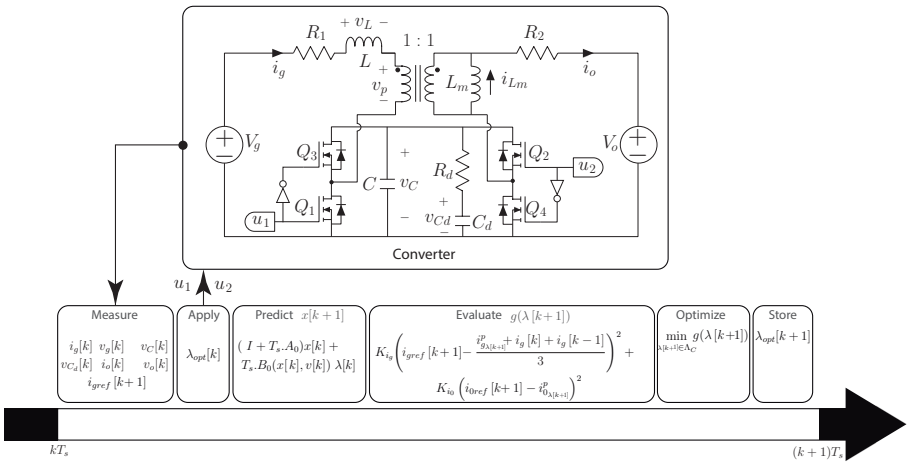

Fig. 5. Time diagram of the execution of the FCS–MPC algorithm.

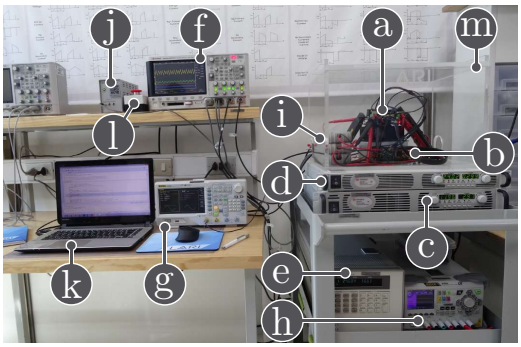

Fig. 6. Experimental configuration for testing the proposed digital current controllers: (a) buck–boost converter, (b) digital signal controller, (c) input dc power supply, (d) output dc power supply, (e) dc electronic load in constant voltage mode, (f) oscilloscope, (g) arbitrary waveform generator to program the analog interface of the input dc power supply, (h) auxiliary power supply for DSC, converter current and voltage sensors and MOSFET Drivers, (i) voltage differential probes, (j) power supply for current probe, (k) laptop for programming the DSC, (l) emergency stop button, (m) acrylic case for testing circuits.

TABLE I
COMPONENTS OF THE TESTED NON-INVERTING BUCK-BOOST CONVERTER

Component	Description	Type
Q_1 to Q_4	Power MOSFETs	IRFB4510PBF
L	SMD Flat Wire Inductor	74435584700, Wurth Elektronik Inductance: 47 μH $\pm$20% DC Resistance: 19.2 $m\Omega$ $\pm$10%
C	Ceramic Capacitor X7R dielectric	CKG57NX7R2A106M500JH, TDK 2 x 10 μF $\pm$20%
R_d	Damping Resistor	0.5 Ω $\pm$0.5%, 1 W, Vishay WSL2512R5000FEA
C_d	Aluminum Electrolytic Capacitor	100 μF $\pm$20%, Panasonic EEEFK2A101AM
L_m	WE-CFWI Coupled Flatwire Inductor	74485540290, Wurth Elektronik Inductance: L_1=L_2=4 x 2.9 μH $\pm$20% Turns ratio: 1 : 1 DC Resistance: R_{DC1}=R_{DC2}=4 x 5.6 $m\Omega$ $\pm$10%

IV. SIMULATION AND EXPERIMENTAL RESULTS

This section discusses the performance of the input current control based on the FCS-MPC (see block diagram of Fig. 5), presented in the previous section in the experimental setup shown in Fig. 6. A prototype of a synchronous noninverting buck–boost converter was built for testing purposes. Its power circuit components are listed in Table I. The converter's control was implemented into a Texas Instruments' TMS320F28335 digital signal controller (DSC) with a 150 MHz clock frequency, a 32-bit CPU, 12-bit ADC and a sampling frequency of 200 kHz that allows a maximum calculation time of 5 μs before the next sampling. The proposed model predictive control strategy reaches a computational burden around 5 μs which is approximately half of the available time. Even though the formulation of the proposed control strategy was done in $k+1$, the real implementation in a digital system considers delay compensation using estimated values for $k+1$ and predictions in $k+2$ [33].

Figs. 7 and 8 show simulated and experimental responses of the converter to reference current i_{ref} variation during operation in both boost and buck modes. For each operating mode, the current reference has been changed from 3 A to 6 A and back to 3 A. In all cases, the input current i_g is well regulated and the transient deviations from the reference are within the desired boundaries with both buck and boost operation modes. It can be observed in Figs. 7 and 8 that the controlled current adequately follows the current reference at all times from the steady–state to the changes in the current reference. In addition, the current reference changes are achieved in a fast manner and without overshoot. Figs. 7(a) and 7(c) have an equivalent switching frequency of 37.20 kHz and 35.71 kHz, respectively. And Fig. 8(a) has an equivalent switching frequency of 34.55 kHz while Fig. 8(c) has a frequency of 35.48 kHz.

Fig. 9 shows the FCS-MPC during the controller start-up in each operation modes (buck and boost) for two different values of i_{ref} (3 A and 6 A). From this figure, it can be concluded that the control starts up in a smooth way and without overshoots

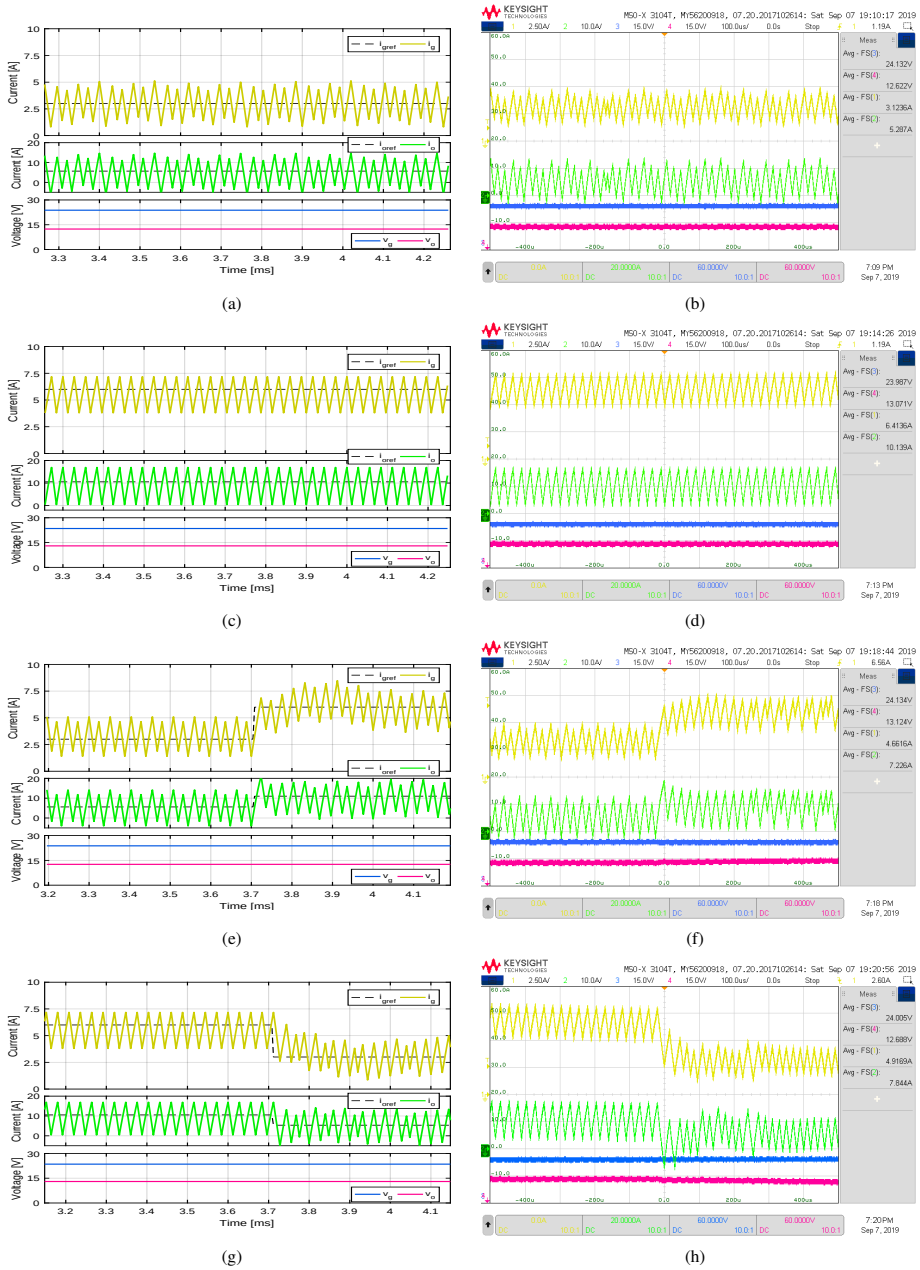

Fig. 7. Simulated (a), (c), (e), (g) and experimental (b), (d), (f), (h) responses of the input current control based on a FCS-MPC strategy when the reference i_{ref}: (a,b) is equal to 3 A, (c,d) is equal to 6 A, (e,f) changes from 3 A to 6 A, and (g,h) from 6 A to 3 A. The converter is operating in buck mode ($V_g = 24$ V and $V_o = 12$ V). CH1: i_g (2.5 A/div), CH2: i_o (10 A/div), CH3: V_g (15 V/div), CH4: V_o (15 V/div) and a time base of 100 μs.

or specific start up codes. The time required to reach the reference with zero initial conditions is around 30 μs in both operation modes (buck and boost). The PSIM simulation and the experimental results are in good agreement as can be seen in all the presented experimental results. The behavior of the input current i_g during these demanding variations confirms the good performance of the proposed digital controller.

The experimental response of the buck–boost regulator to a low-frequency triangular input voltage going from 14.5 V to 21.5 V is depicted in Fig. 10 where the waveform of the input voltage V_g, output voltage V_o, input current i_g, and output current could be compared with their corresponding simulation. In this experiment the output voltage V_o is 18.0 V which corresponds with the average value of the input voltage to ensure an operation in boost and buck modes. It is important to note that no transition technique between the operation modes (boost or buck) is being used in the current control proposed in this article. However, the input current i_g is well regulated ($i_{ref} = 6$ A) and exhibits a smooth behavior in all the transitions between modes. These good results are due to the use of the same controller in all the operation modes and the fact that during the transition there are no extreme cycles because the control technique is of variable frequency. Finally, a comparison between the model predictive control approach with a conventional linear method is addressed in this section. The linear current loop compensator $G_c(s)$ is

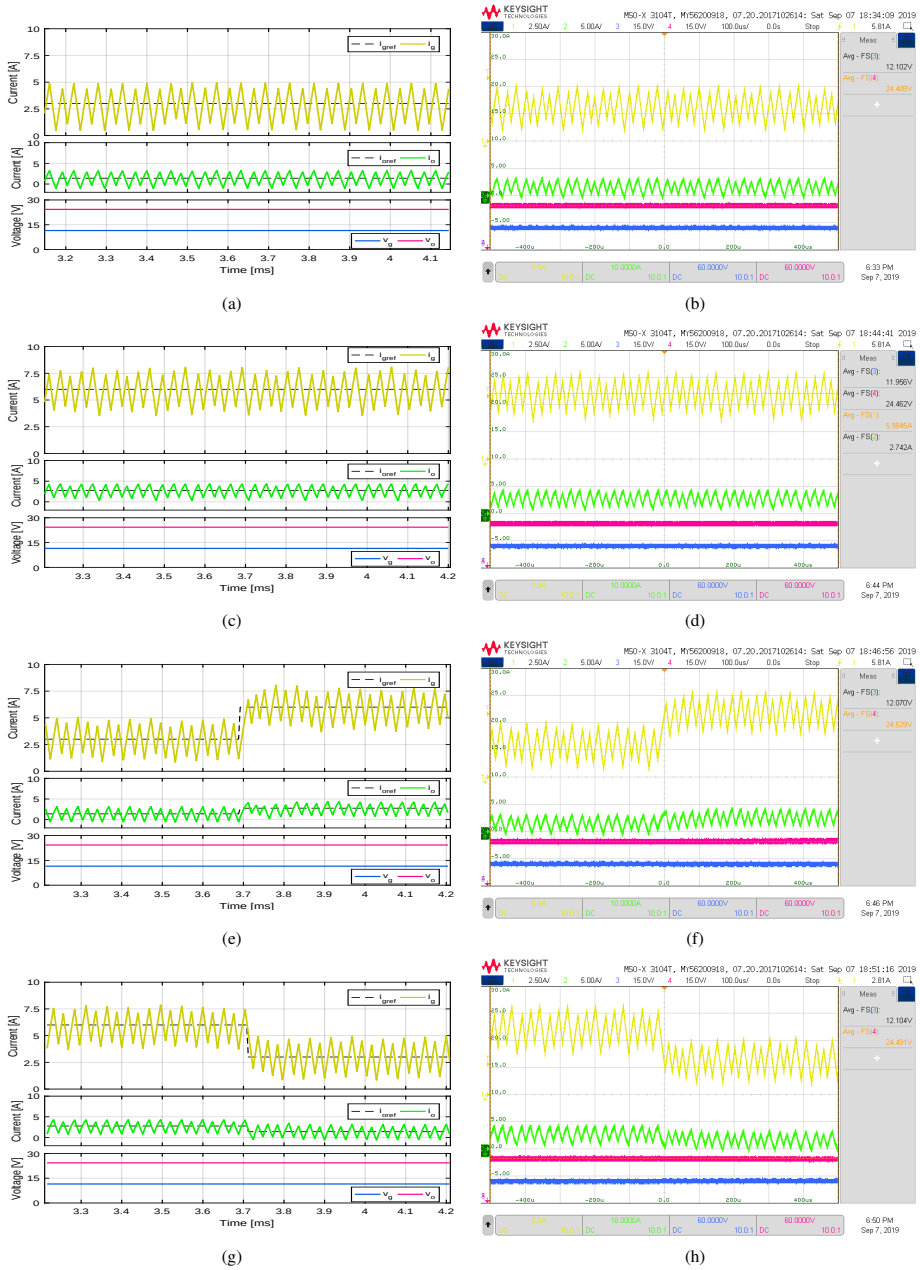

Fig. 8. Simulated (a), (c), (e), (g) and experimental (b), (d), (f), (h) responses of the input current control based on a FCS-MPC strategy when the reference i_{ref}: (a,b) is equal to 3 A, (c,d) is equal to 6 A, (e,f) changes from 3 A to 6 A, and (g,h) from 6 A to 3 A. The converter is operating in boost mode ($V_g = 12$ V and $V_o = 24$ V). CH1: i_g (2.5 A/div), CH2: i_o (5 A/div), CH3: V_g (15 V/div), CH3: V_o (15 V/div) and a time base of 100 μs.

designed using a lag network with a high frequency pole as proposed in [34]. On the one hand, there are different reported criteria to place the high frequency pole, for example in [35] it is recommend to place it between one-third and one-half of the switching frequency to attenuate switching noise while in [36] it is suggested to place this pole above half of the switching frequency. The intersection of both criteria results in a pole at half of the switching frequency. On the other hand, the low frequency pole of the compensator has been placed at the origin which allows to eliminate the steady-state error [37]. In [36], it is recommended to place the zero at least one decade below half the switching frequency. Therefore, the zero was placed at a tenth of the high frequency pole and the compensator gain was adjusted through different simulations to ensure wide bandwidth and a minimum phase margin of 45^o. For a fair comparison purposes between both control strategies is selecting a switching frequency of 50 kHz for the design of the second order compensator transfer function, this is

$$G_c(s) = K\frac{(\tau_2 s + 1)}{s(\tau_1 s + 1)} \tag{17}$$

where the compensator parameters have been selected as follows: $\tau_1 = 3.18\,\mu$s, $\tau_2 = 66\,\mu$s, and $K = 1500\,(sA)^{-1}$. A bilinear transformation is used to estimate the transformation from continuous to discrete of the compensator (17), which results in the following discrete-time transfer function

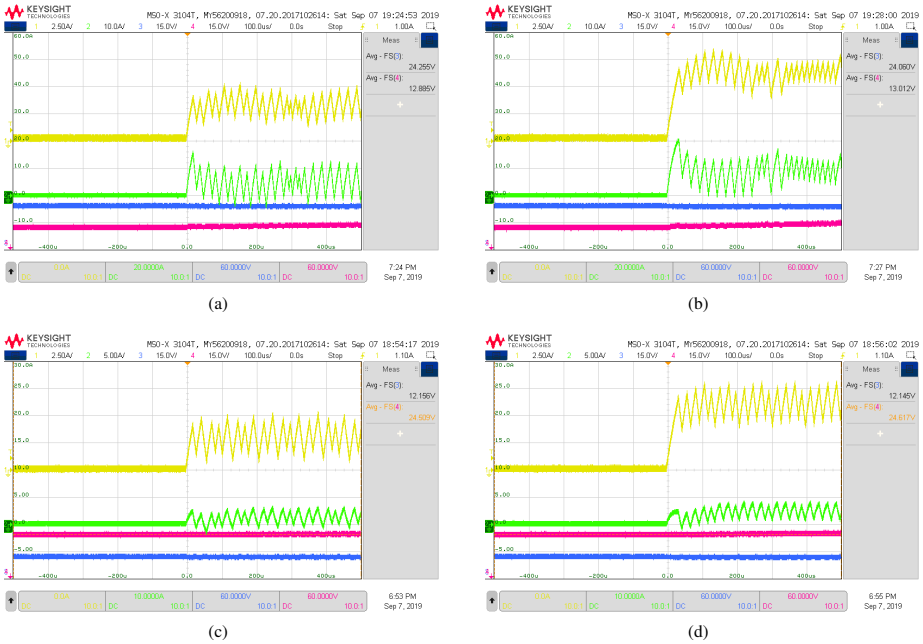

Fig. 9. Experimental results of converter start-up. In: (a) buck mode i_{ref} equal to 3 A, (b) buck mode i_{ref} equal to 6 A, (c) boost mode i_{ref} equal to 3 A, and (d) boost mode i_{ref} equal to 6 A. CH1: i_g (2.5 A/div), CH2: i_o (5/10 A/div), CH3: V_g (15 V/div), CH4: V_o (15 V/div) and a time base of 100 μs.

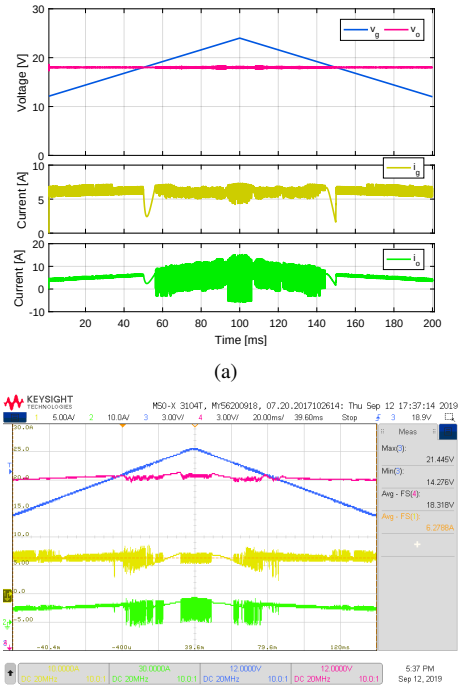

(a)

(b)

Fig. 10. Simulated (a) and Experimental (b) results of transition between buck and boost operating modes. In this experiment V_g is 5 Hz triangular wave going from 14.5 V to 21.5 V, $V_o = 18$ V, and i_{ref} equal to 6 A. CH1: i_g (5 A/div), CH2: i_o (10 A/div), CH3: V_g (3 V/div), CH4: V_o (3 V/div) and a time base of 20 ms.

$$G_c(z) = \frac{0.08649z^2 + 0.02276z - 0.06373}{z^2 - 0.4825z - 0.5175} \tag{18}$$

Once the digital control based on a linear technique and operating at a frequency equivalent to that of the MPC has been designed, it is time to compare both techniques. Fig. 11 shows a simulation comparison between both digital control strategies which includes a start-up at 1 ms and a current reference change from 6 A to 3 A at 2 ms. In boost mode, the PI based control has a i_g maximum current (I_{peak}) during the start-up of 8.55 A while the FSC-MPC has a I_{peak} of 6.76 A as shown in Fig. 11. In buck mode, the I_{peak} corresponds to 19.33 A for the PI control while for the FSC-MPC has a value of 7.08 A. This high starting current in the PI control can be dangerous for converter components and explains the need to use a start-up algorithm. Therefore, during the converter start-up the proposed FSC-MPC strategy presents a superior behavior than a linear technique as it does not require startup algorithms since it can operate in a wide range of operating points. Besides, the time elapsed from the control start-up until the current (i_g) reaches the average value of the current reference (i_{gref}) named t_{su} is much less in the FSC-MPC than in the PI control for both modes (boost and buck). In the case of the buck mode, t_{su} is of 0.32 ms with a PI control while with the FSC-MPC strategy a time of 0.08 ms is reached. And in the case of the boost mode, t_{su} is of 0.22 ms and 0.06 ms for the PI control and the FSC-MPC strategy respectively. Therefore, the proposed FSC-MPC technique exhibits much faster behavior than its linear counterpart. This is also evident when t_{ref} is calculated. This time corresponds to the time elapsed since a current reference change (in 2 ms) until i_g reaches the average value of the current. In buck mode t_{ref} is equal to 0.16 ms and 0.05 ms for the PI strategy and the FSC-MPC respectively. Finally, in the case of a boost mode t_{ref} is equal to 0.22 ms and 0.06 ms for the PI control and FSC-MPC respectively. Therefore, the MPC strategy was superior with the lower current peaks during the start-up and the faster time

to reach the reference during the start-up and current reference changes in comparison with the linear proposed control as shown in Fig. 11.

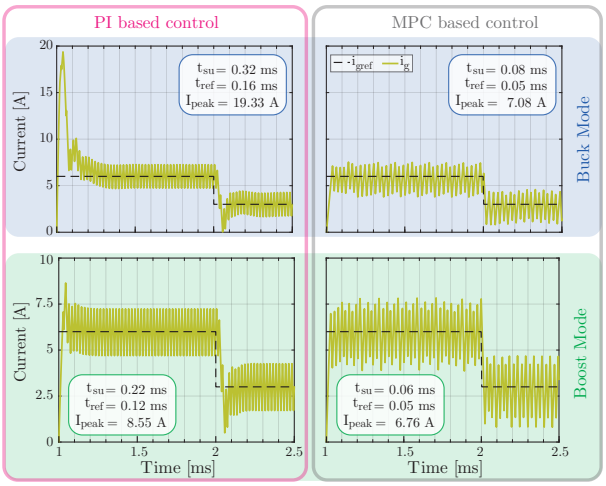

Fig. 11. Comparison of a PI based and the proposed MPC strategies operating in boost and buck mode.

Finally, a sensitivity analysis is performed to study the impact of the parameter detuning in the proposed FSC-MPC strategy. According to the Table I the inductor L has a inductance of 47 μH with a tolerance of $\pm 20\%$, the coupled inductor L_m has a inductance of 11.6 μH with a tolerance of $\pm 20\%$, the capacitor C has a capacitance of 20 μF with a tolerance of $\pm 20\%$, the damping capacitor C_d has a capacitance of 100 μF with a tolerance of $\pm 20\%$, and the damping resistor R_d has a resistance of 0.5 Ω with a tolerance of $\pm 0.5\%$. To reproduce the parameter detuning, parameters in the predictive model (L, L_m, C, C_d and R_d) are varied one at a time according to the tolerance, in order to investigate the individual effect of each parameter in the performance of the $MAPE(i_g)$. This measure corresponds to the mean absolute percentage error between the input current i_g and its respective reference i_{gref}. Therefore, a sensitivity analysis of each converter parameter operating in boost mode (V_g = 12 V and V_o = 24 V) and buck mode (V_g = 24 V and V_o = 12 V) both with a i_{gref} =6 A is shown in Fig. 12. From the obtained results it can be stated that L has a significant impact in the input current tracking error when the inductance tolerance has values around $\pm 20\%$. However, even in the worst case the $MAPE(i_g)$ has a small variation of 3.6% in buck mode and 4.0% in boost mode. On the other hand, it is evident that the detuning of the other variables of the converter (L_m, C, C_d and R_d) do not have a relevant effect on the $MAPE(i_g)$ as shown in Fig. 12. Another sensitivity analysis corresponds to the output current reference i_{0ref} used in the cost function (13) and presented in (14). According to (14), this current reference depends on the converter parameters R_1 and R_2. In this case, R_1 and R_2 are simultaneously varied with a tolerance of $\pm 10\%$ with respect to their nominal values (R_1 = 41.6mΩ and R_2 = 22.4mΩ). Surface plots shown in Fig. 13 represent the $MAPE(i_g)$ error in the considered operating points which corresponds to a boost mode (V_g = 12 V and V_o = 24 V) and buck mode (V_g = 24 V and V_o = 12 V) both with a i_{gref} =6 A. It can be concluded from the obtained results that R_1 and R_2 has not a significant impact in the current control performance. This behaviour can be explained by the small values of these equivalent resistances and by the fact that $K_{i_g} >> K_{i_0}$ in (13).

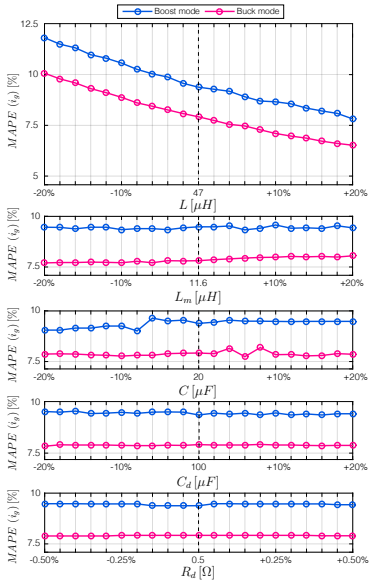

Fig. 12. Sensitivity analysis of the converter parameters (L, L_m, C, C_d and R_d) operating in boost mode (V_g = 12 V and V_o = 24 V) and buck mode (V_g = 24 V and V_o = 12 V) both with a i_{gref} =6 A.

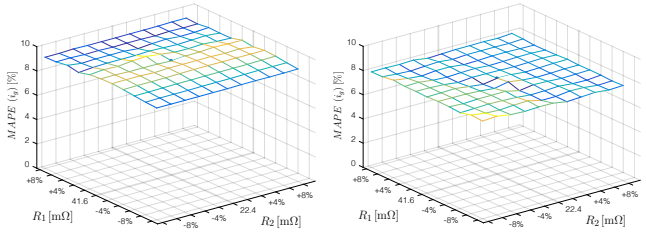

(a) (b)

Fig. 13. Sensitivity analysis for simultaneous R_1 and R_2 variation for: (a) buck mode (V_g = 24 V and V_o = 12 V), (b) boost mode (V_g = 12 V and V_o = 24 V).

V. Conclusion

In this paper, a FCS-MPC is used to regulate the input current of the versatile buck-boost converter in an extended operation range. Cost function includes voltage and currents measurements and weighting factors set to control the dynamic response. In each iteration, valid states of a switching table are evaluated, according to operation in buck or boost mode. The controller selects the state that minimizes the cost function which will be applied at the end of the next sampling period. Tests in buck, boost and buck-boost modes with different operation points show that proposed nonlinear control enhance the converter's performance in comparison with the results of linear control strategies. In addition, a sensitivity analysis shows that the current control performance has a relative dependency with the estimate of the input inductor L while the other converter components detuning does not have a

considerable effect on the control. Main features of FCS-MPC are low computational cost, high accuracy current tracking and smooth transitions between buck and boost modes. This control strategy is recommended for other dc-dc converters due to its simplicity and performance. Future works will make an experimental verification of the versatile buck-boost converter with the proposed controller in a single-phase rectifier application.

APPENDIX
VERSATILE BUCK-BOOST CONVERTER MODEL

Let us consider the bidirectional buck–boost converter with magnetic coupling between the input and output inductors, RC type damping network, and coupled inductors turns ratio 1:1 shown in Fig. 1. In this section are presented different models with the goal of studying their set of equilibria and the natural constraint on the converter internal variables. Applying the fundamental Kirchhoff laws to the converter shown in Fig. 1, we obtain

$$\begin{cases} V_0(t) + R_2 i_0(t) + L_m \dfrac{di_{L_m}(t)}{dt} - u_2(t) v_c(t) = 0 \\ -(i_g(t) + i_{L_m}(t)) u_2(t) - \dfrac{v_c(t) - v_{C_d}(t)}{R_d} + (1 - u_1(t)) i_g(t) \\ = C \dfrac{dv_c(t)}{dt} \\ \dfrac{v_c(t) - v_{C_d}(t)}{R_d} = C_d \dfrac{dv_{C_d}(t)}{dt} \\ V_g(t) - R_1 i_g(t) - L \dfrac{di_g(t)}{dt} + v_p(t) - (1 - u_1(t)) v_c(t) = 0 \\ -V_0(t) + u_2(t) v_c(t) - R_2 i_0(t) = v_p(t) \end{cases} \tag{A.1}$$

where $(u_1(t), u_2(t)) \in \{0,1\}^2$.

Remarking that $i_0 = i_g + i_{L_m}$, we have

$$\begin{aligned} \frac{di_0(t)}{dt} &= \tfrac{1}{L}(V_g(t) - R_1 i_g(t) - (1 - u_1(t)) v_c(t) - V_0(t) \\ &\quad + u_2(t) v_c(t) - R_2 i_0(t)) \\ &\quad + \frac{1}{L_m}(-V_0(t) - R_2 i_0(t) + u_2(t) v_c(t)) \end{aligned} \tag{A.2}$$

If we define the state vector as $x(t) = [i_g(t), i_0(t), v_c(t), v_{C_d}(t)]^T$ and the vector $v(t) = [V_g(t), V_0(t)]^T$, we have the model (A.3). It can also be written as

$$\begin{aligned} \frac{dx(t)}{dt} &= (A_0 + A_{u_1} u_1(t) + A_{u_2} u_2(t))\, x(t) + B v(t) \\ &= \left(A_0 + A_{u_1(t) u_2(t)}\right) x(t) + B v(t) \end{aligned} \tag{A.4}$$

with $A_{u_1(t)u_2(t)} = A_{u_1} u_1(t) + A_{u_2} u_2(t)$, $(u_1(t), u_2(t)) \in \{0,1\}^2$ and

$$A_0 = \begin{bmatrix} -\dfrac{R_1}{L} & -\dfrac{R_2}{L} & -\dfrac{1}{L} & 0 \\ -\dfrac{R_1}{L} & -\dfrac{R_2}{L} - \dfrac{R_2}{L_m} & -\dfrac{1}{L} & 0 \\ \dfrac{1}{C} & 0 & -\dfrac{1}{R_d C} & \dfrac{1}{R_d C} \\ 0 & 0 & \dfrac{1}{R_d C_d} & -\dfrac{1}{R_d C_d} \end{bmatrix} \tag{A.5}$$

$$A_{u_1} = \begin{bmatrix} 0 & 0 & \dfrac{1}{L} & 0 \\ 0 & 0 & \dfrac{1}{L} & 0 \\ -\dfrac{1}{C} & 0 & 0 & 0 \\ 0 & 0 & 0 & 0 \end{bmatrix} \tag{A.6}$$

$$A_{u_2} = \begin{bmatrix} 0 & 0 & \dfrac{1}{L} & 0 \\ 0 & 0 & \dfrac{1}{L} + \dfrac{1}{L_m} & 0 \\ 0 & -\dfrac{1}{C} & 0 & 0 \\ 0 & 0 & 0 & 0 \end{bmatrix} \tag{A.7}$$

$$B = \begin{bmatrix} \dfrac{1}{L} & -\dfrac{1}{L} \\ \dfrac{1}{L} & -\dfrac{1}{L} - \dfrac{1}{L_m} \\ 0 & 0 \\ 0 & 0 \end{bmatrix} \tag{A.8}$$

We can write $A_{u_1(t)u_2(t)}$ as

$$\begin{aligned} A_{u_1(t)u_2(t)} = \quad & (1 - u_1(t))(1 - u_2(t)) A_{00} + u_1(t) u_2(t) A_{11} \\ & + u_1(t)(1 - u_2(t)) A_{10} + (1 - u_1(t)) u_2(t) A_{01} \end{aligned}$$

with

$$\begin{aligned} A_{00} \triangleq A_1 = 0,\ A_{01} \triangleq A_2 = A_{u_2},\ A_{10} \triangleq A_3 = A_{u_1} \\ \text{and } A_{11} \triangleq A_4 = A_{u_1} + A_{u_2} \end{aligned} \tag{A.9}$$

$u_1(t)$ and $u_2(t)$ are the control variables. We introduce the functions $\lambda_i(t),\ i = 1, \cdots, 4$ associated with, respectively, matrices $A_i,\ i = 1, \cdots, 4$ and defined by

$$\lambda_1(t) = (1 - u_1(t))(1 - u_2(t)),\ \lambda_2(t) = (1 - u_1(t)) u_2(t),$$
$$\lambda_3(t) = u_1(t)(1 - u_2(t)) \text{ and } \lambda_4(t) = u_1(t) u_2(t)$$

We have

$$\sum_{i=1}^{4} \lambda_i(t) = (1 - u_1(t) + u_1(t))(1 - u_2(t) + u_2(t)) = 1 \tag{A.10}$$

Then model (A.4) can also be written

$$\frac{dx(t)}{dt} = A_0 x(t) + B_0(x(t), v(t)) \lambda(t) \tag{A.11}$$

where A_0 is defined above and

$$\begin{aligned} B_0(x(t), v(t)) = [A_1 x(t) + B v(t), A_2 x(t) + B v(t) \\ A_3 x(t) + B v(t), A_4 x(t) + B v(t)] \end{aligned} \tag{A.12}$$

with $\lambda : \mathbb{R} \to \Lambda_S,\ \Lambda_S = \left\{\theta \in \{0,1\}^4 : \sum_{i=1}^4 \theta_i = 1\right\}$. Note that now $\lambda(t)$ is the control vector. Associated with the previous model, a model called "relaxed" or "embedded" is introduced. The difference with model (A.11) is that for the relaxed model $\lambda : \mathbb{R} \to \Lambda_R,\ \Lambda_R = \left\{\theta \in [0,1]^4 : \sum_{i=1}^4 \theta_i = 1\right\}$. The interest of such a model is that for arbitrary close initial conditions, the solution of initial value problems for model (A.11) is dense in the solution set of initial value problems of the relaxed model for an appropriate topology (C^0 Whitney

$$\frac{dx(t)}{dt} = \begin{bmatrix} -\frac{R_1}{L} & -\frac{R_2}{L} & -\frac{(1-u_1(t)-u_2(t))}{L} & 0 \\ -\frac{R_1}{L} & -\frac{R_2}{L}-\frac{R_2}{L_m} & -\frac{(1-u_1(t)-u_2(t))}{L}+\frac{u_2(t)}{L_m} & 0 \\ \frac{1-u_1(t)}{C} & -\frac{u_2(t)}{C} & -\frac{1}{R_dC} & \frac{1}{R_dC} \\ 0 & 0 & \frac{1}{R_dC_d} & -\frac{1}{R_dC_d} \end{bmatrix} x(t) + \begin{bmatrix} \frac{1}{L} & -\frac{1}{L} \\ \frac{1}{L} & -\frac{1}{L}-\frac{1}{L_m} \\ 0 & 0 \\ 0 & 0 \end{bmatrix} v(t) \tag{A.3}$$

$$\frac{d\underline{x}(t)}{dt} = \begin{bmatrix} -\frac{R_1}{L}-\frac{R_2}{L} & -\frac{R_2}{L} & -\frac{1-u_1(t)-u_2(t)}{L} & 0 \\ -\frac{R_2}{L_m} & -\frac{R_2}{L_m} & \frac{u_2(t)}{L_m} & 0 \\ \frac{1-u_1(t)-u_2(t)}{C} & -\frac{u_2(t)}{C} & -\frac{1}{R_dC} & \frac{1}{R_dC} \\ 0 & 0 & \frac{1}{R_dC_d} & -\frac{1}{R_dC_d} \end{bmatrix} \underline{x}(t) + \begin{bmatrix} \frac{1}{L} & -\frac{1}{L} \\ 0 & -\frac{1}{L_m} \\ 0 & 0 \\ 0 & 0 \end{bmatrix} v(t) \tag{A.13}$$

topology on infinite intervals $[0,\infty)$), see [38] for details. This connection can also be examined by studying the nature of solutions of initial values problems of model (A.11) (see [39] or [40] for details). This connection has important practical implications, among the most important: it is possible to approximate trajectories of the relaxed model (non switching model) by trajectories of switching model (A.11). In particular, if a set of equilibria exists for the relaxed model, each of them can be approximated by an appropriate switching control law $\lambda : \mathbb{R} \to \Lambda_S$ applied to (A.11). This last remark motivates the interest for a study of the nature and the complete characterization of a set of equilibria of the relaxed model. One of the main interest of the converter under study is its versatility. But the counterpart of such a flexibility is a certain difficulty for the determination of the control laws associated with each operation mode.

In order to easily analyze in some cases the converter operation, another model deduced from (A.11) can be derived. it is obtained by introducing a new state vector

$$\underline{x} = [i_g(t), i_0(t) - i_g(t), v_c(t), v_{C_d}(t)]^T$$

which leads to the model (Model 2) presented in (A.13).This model can also be written as

$$\begin{aligned} \frac{d\underline{x}(t)}{dt} &= \left(\underline{A_0} + \underline{A_{u_1}}u_1(t) + \underline{A_{u_2}}u_2(t)\right)x(t) + \underline{B}v(t) \\ &= \left(\underline{A_0} + \underline{A}_{u_1(t)u_2(t)}\right)x(t) + \underline{B}v(t) \end{aligned} \tag{A.14}$$

with $\underline{A}_{u_1(t)u_2(t)} = \underline{A_{u_1}}u_1(t) + \underline{A_{u_2}}u_2(t),\ (u_1(t),u_2(t)) \in \{0,1\}^2$ and

$$\underline{A_0} = \begin{bmatrix} -\frac{R_1}{L}-\frac{R_2}{L} & -\frac{R_2}{L} & -\frac{1}{L} & 0 \\ -\frac{R_2}{L_m} & -\frac{R_2}{L_m} & 0 & 0 \\ \frac{1}{C} & 0 & -\frac{1}{R_dC} & \frac{1}{R_dC} \\ 0 & 0 & \frac{1}{R_dC_d} & -\frac{1}{R_dC_d} \end{bmatrix} \tag{A.15}$$

$$\underline{A_{u_1}} = \begin{bmatrix} 0 & 0 & \frac{1}{L} & 0 \\ 0 & 0 & 0 & 0 \\ -\frac{1}{C} & 0 & 0 & 0 \\ 0 & 0 & 0 & 0 \end{bmatrix} \tag{A.16}$$

$$\underline{A_{u_2}} = \begin{bmatrix} 0 & 0 & \frac{1}{L} & 0 \\ 0 & 0 & \frac{1}{L_m} & 0 \\ -\frac{1}{C} & -\frac{1}{C} & 0 & 0 \\ 0 & 0 & 0 & 0 \end{bmatrix} \tag{A.17}$$

$$\underline{B} = \begin{bmatrix} \frac{1}{L} & -\frac{1}{L} \\ 0 & -\frac{1}{L_m} \\ 0 & 0 \\ 0 & 0 \end{bmatrix} \tag{A.18}$$

This last model can be used to easily deduced the power balance for the converter. It is obtained multiplying on the left the dynamical equation by

$$\begin{bmatrix} Li_g(t) & L_m(i_0(t)-i_g(t)) & Cv_c(t) & C_dv_{C_d}(t) \end{bmatrix}$$

leading to

$$\begin{aligned} Li_g(t)\frac{di_g(t)}{dt} + L_mi_0(t)\frac{di_0(t)}{dt} - L_mi_0(t)\frac{di_g(t)}{dt} - \\ L_mi_g(t)\frac{di_0(t)}{dt} + L_mi_g(t)\frac{di_g(t)}{dt} + Cv_c(t)\frac{dv_c(t)}{dt} \\ +C_dv_{C_d}(t)\frac{dv_{C_d}(t)}{dt} = -R_1i_g(t)^2 - R_2i_0(t)^2 - \\ \frac{(v_C(t)-v_{C_d}(t))^2}{R_d} + V_g(t)i_g(t) - V_0(t)i_0(t) \end{aligned} \tag{A.19}$$

The previous balance equation is always satisfied and can be seen as a natural constraint on the converter internal variables.

REFERENCES

[1] S. Kouro, M. A. Perez, J. Rodriguez, A. M. Llor, and H. A. Young, "Model predictive control: Mpc's role in the evolution of power electronics," *IEEE Industrial Electronics Magazine*, vol. 9, no. 4, pp. 8–21, Dec 2015.

[2] P. G.-T. no, J. P. Torreglosa, L. M. Fernández-Ramírez, and F. Jurado, "Decentralized fuzzy logic control of microgrid for electric vehicle charging station," *IEEE Journal of Emerging and Selected Topics in Power Electronics*, vol. 6, no. 2, pp. 726–737, January 2018.

[3] M. Rakhshan, N. Vafamand, M. H. Khooban, and F. Blaabjerg, "Maximum power point tracking control of photovoltaic systems: A polynomial fuzzy model-based approach," *IEEE Journal of Emerging and Selected Topics in Power Electronics*, vol. 6, no. 1, pp. 292–299, March 2018.

[4] L. Zheng, F. Jiang, J. Song, Y. Gao, and M. Tian, "A discrete time repetitive sliding mode control for voltage source inverters," *IEEE Journal of Emerging and Selected Topics in Power Electronics*, vol. PP, no. 99, pp. 1–1, 2017.

[5] M. Zhang, Y. Li, F. Liu, L. Luo, Y. Cao, and M. Shahidehpour, "Voltage stability analysis and sliding-mode control method for rectifier in dc systems with constant power loads," *IEEE Journal of Emerging and Selected Topics in Power Electronics*, vol. 5, no. 4, pp. 1621–1630, Dec 2017.

[6] F. Sebaaly, H. Vahedi, H. Y. Kanaan, N. Moubayed, and K. Al-Haddad, "Sliding mode fixed frequency current controller design for grid-connected npc inverter," *IEEE Journal of Emerging and Selected Topics in Power Electronics*, vol. 4, no. 4, pp. 1397–1405, Dec 2016.

[7] Y. A. Zúñiga-Ventura, D. Langarica-Córdoba, J. Leyva-Ramos, L. H. Díaz-Saldierna, and V. M. Ramírez-Rivera, "Adaptive backstepping control for a fuel cell/boost converter system," *IEEE Journal of Emerging and Selected Topics in Power Electronics*, vol. 6, no. 2, pp. 686–695, June 2018.

[8] E. Z. Bighash, S. M. Sadeghzadeh, E. Ebrahimzadeh, and F. Blaabjerg, "Adaptive harmonic compensation in residential distribution grid by roof-top pv systems," *IEEE Journal of Emerging and Selected Topics in Power Electronics*, vol. PP, no. 99, pp. 1–1, 2018.

[9] S. Kouro, P. Cortes, R. Vargas, U. Ammann, and J. Rodriguez, "Model predictive control–a simple and powerful method to control power converters," *IEEE Transactions on Industrial Electronics*, vol. 56, no. 6, pp. 1826–1838, June 2009.

[10] S. Vazquez, J. I. Leon, L. G. Franquelo, J. Rodriguez, H. A. Young, A. Marquez, and P. Zanchetta, "Model predictive control: A review of its applications in power electronics," *IEEE Industrial Electronics Magazine*, vol. 8, no. 1, pp. 16–31, March 2014.

[11] F. Donoso, A. Mora, R. Cárdenas, A. Angulo, D. Sáez, and M. Rivera, "Finite-set model-predictive control strategies for a 3l-npc inverter operating with fixed switching frequency," *IEEE Transactions on Industrial Electronics*, vol. 65, no. 5, pp. 3954–3965, May 2018.

[12] S. Vazquez, J. Rodriguez, M. Rivera, L. G. Franquelo, and M. Norambuena, "Model predictive control for power converters and drives: Advances and trends," *IEEE Transactions on Industrial Electronics*, vol. 64, no. 2, pp. 935–947, Feb 2017.

[13] L. Tarisciotti, J. Lei, A. Formentini, A. Trentin, P. Zanchetta, P. Wheeler, and M. Rivera, "Modulated predictive control for indirect matrix converter," *IEEE Transactions on Industry Applications*, vol. 53, no. 5, pp. 4644–4654, Sept 2017.

[14] V. Yaramasu, B. Wu, M. Rivera, and J. Rodriguez, "A new power conversion system for megawatt pmsg wind turbines using four-level converters and a simple control scheme based on two-step model predictive strategy–part i: Modeling and theoretical analysis," *IEEE Journal of Emerging and Selected Topics in Power Electronics*, vol. 2, no. 1, pp. 3–13, March 2014.

[15] ——, "A new power conversion system for megawatt pmsg wind turbines using four-level converters and a simple control scheme based on two-step model predictive strategy–part ii: Simulation and experimental analysis," *IEEE Journal of Emerging and Selected Topics in Power Electronics*, vol. 2, no. 1, pp. 14–25, March 2014.

[16] P. Cortes, M. P. Kazmierkowski, R. M. Kennel, D. E. Quevedo, and J. Rodriguez, "Predictive control in power electronics and drives," *IEEE Transactions on Industrial Electronics*, vol. 55, no. 12, pp. 4312–4324, Dec 2008.

[17] F. Zhang, W. Li, and G. Joós, "A voltage-level-based model predictive control of modular multilevel converter," *IEEE Transactions on Industrial Electronics*, vol. 63, no. 8, pp. 5301–5312, Aug 2016.

[18] Y. Zhang, X. Wu, X. Yuan, Y. Wang, and P. Dai, "Fast model predictive control for multilevel cascaded h-bridge statcom with polynomial computation time," *IEEE Transactions on Industrial Electronics*, vol. 63, no. 8, pp. 5231–5243, Aug 2016.

[19] M. Mazuela, I. Baraia, A. Sanchez-Ruiz, I. Echeverria, I. Torre, and I. Atutxa, "Dc-link voltage balancing strategy based on svm and reactive power exchange for a 5l-mpc back-to-back converter for medium-voltage drives," *IEEE Transactions on Industrial Electronics*, vol. 63, no. 12, pp. 7864–7875, Dec 2016.

[20] L. Cheng, P. Acuna, R. P. Aguilera, J. Jiang, S. Wei, J. Fletcher, and D. D. C. Lu, "Model predictive control for dc-dc boost converters with reduced-prediction horizon and constant switching frequency," *IEEE Transactions on Power Electronics*, vol. PP, no. 99, pp. 1–1, 2017.

[21] J. Saeed and A. Hasan, "Unit prediction horizon binary search-based model predictive control of full-bridge dc–dc converter," *IEEE Transactions on Control Systems Technology*, vol. 26, no. 2, pp. 463–474, March 2018.

[22] L. Cavanini, G. Cimini, G. Ippoliti, and A. Bemporad, "Model predictive control for pre-compensated voltage mode controlled dc–dc converters," *IET Control Theory Applications*, vol. 11, no. 15, pp. 2514–2520, 2017.

[23] S. Mariethoz, S. Almer, M. Baja, A. G. Beccuti, D. Patino, A. Wernrud, J. Buisson, H. Cormerais, T. Geyer, H. Fujioka, U. T. Jonsson, C. Y. Kao, M. Morari, G. Papafotiou, A. Rantzer, and P. Riedinger, "Comparison of hybrid control techniques for buck and boost dc-dc converters," *IEEE Transactions on Control Systems Technology*, vol. 18, no. 5, pp. 1126–1145, Sept 2010.

[24] T. Geyer, G. Papafotiou, and M. Morari, "Hybrid model predictive control of the step-down dc–dc converter," *IEEE Transactions on Control Systems Technology*, vol. 16, no. 6, pp. 1112–1124, Nov 2008.

[25] P. Karamanakos, T. Geyer, and S. Manias, "Direct model predictive current control of dc-dc boost converters," in *2012 15th International Power Electronics and Motion Control Conference (EPE/PEMC)*, Sept 2012, pp. DS2c.11–1–DS2c.11–8.

[26] C. Restrepo, J. Calvente, A. Cid-Pastor, A. E. Aroudi, and R. Giral, "A noninverting buck–boost dc–dc switching converter with high efficiency and wide bandwidth," *IEEE Transactions on Power Electronics*, vol. 26, no. 9, pp. 2490–2503, Sept 2011.

[27] H. Ramírez-Murillo, C. Restrepo, T. Konjedic, J. Calvente, A. Romero, C. R. Baier, and R. Giral, "An efficiency comparison of fuel-cell hybrid systems based on the versatile buck–boost converter," *IEEE Transactions on Power Electronics*, vol. 33, no. 2, pp. 1237–1246, Feb 2018.

[28] H. Ramírez-Murillo, C. Restrepo, J. Calvente, A. Romero, and R. Giral, "Energy management of a fuel-cell serial–parallel hybrid system," *IEEE Transactions on Industrial Electronics*, vol. 62, no. 8, pp. 5227–5235, Aug 2015.

[29] ——, "Energy management dc system based on current-controlled buck-boost modules," *IEEE Transactions on Smart Grid*, vol. 5, no. 5, pp. 2644–2653, Sept 2014.

[30] C. Restrepo, J. Calvente, A. Romero, E. Vidal-Idiarte, and R. Giral, "Current-Mode Control of a Coupled-Inductor Buck–Boost DC–DC Switching Converter," *IEEE Transactions on Power Electronics*, vol. 27, no. 5, pp. 2536–2549, May 2012.

[31] C. Restrepo, T. Konjedic, J. Calvente, M. Milanovic, and R. Giral, "Fast transitions between current control loops of the coupled-inductor buck–boost dc–dc switching converter," *IEEE Transactions on Power Electronics*, vol. 28, no. 8, pp. 3648–3652, Aug 2013.

[32] C. Restrepo, T. Konjedic,J. Calvente, R. Giral, and S. Member, "Hysteretic transition method for avoiding the dead-zone effect and subharmonics in a non-inverting buck-boost converter," *IEEE Transactions on Power Electronics*, vol. 30, no. 6, pp. 1–1, 2014.

[33] P. Cortes, J. Rodriguez, C. Silva, and A. Flores, "Delay compensation in model predictive current control of a three-phase inverter," *IEEE Transactions on Industrial Electronics*, vol. 59, no. 2, pp. 1323–1325, Feb 2012.

[34] J. Sun and R. Bass, "Modeling and practical design issues for average current control," in *Proc. 14th IEEE Appl. Power Electron. Conf. Expo., APEC*, vol. 2, Mar. 1999, pp. 980 –986 vol.2.

[35] P. Cooke, "Modeling average current mode control [of power convertors]," in *Proc. 15th IEEE Appl. Power Electron. Conf. Expo., APEC*, vol. 1, 2000, pp. 256 –262 vol.1.

[36] W. Tang, F. Lee, and R. Ridley, "Small-signal modeling of average current-mode control," *IEEE Trans. Power Electron.*, vol. 8, no. 2, pp. 112 –119, apr 1993.

[37] T. Instruments, "Designing with the TL5001 PWM controller," Texas Instruments, Aplication Report SLVA034A, 1995.

[38] B. Ingalls and E. Sontag, "An Infinite-Time Relaxation Theorem for Differentia Inclusions," *Proceedings of the American Mathematical Society (AMS)*, vol. 131, no. 2, pp. 487–499, 2003.
[39] S. Bengea and R. D. Carlo, "Optimal Control of Switching Systems," *Automatica*, vol. 41, no. 1, pp. 11–27, 2005.
[40] A. F. Filippov, *Differential Equations with Discontinuous Righthand Sides*. Kluwer Academic Press, 2010.

Carlos Restrepo received the Bachelor degree (with honors) and the Master degree in electrical engineering in 2006 and 2007, respectively, from the Universidad Tecnológica de Pereira, Colombia, and the Master degree and the Ph.D. (with honors) degree in electronic engineering from the Universitat Rovira i Virgili de Tarragona, Tarragona, Spain, in 2008 and 2012, respectively. He was a visiting scholar at the Faculty of Electrical Engineering and Computer Science, University of Maribor, Slovenia, in 2011. During 2013 and 2014, he was a Postdoctoral Researcher with the Electrical Power Processing Group, Delft University of Technology, Delft, The Netherlands. From 2014 to 2016 he was a Professor with the Departamento de Ingeniería Eléctrica, Universidad Técnica Federico Santa María, Santiago de Chile, Chile. He is currently a Professor with the Departamento de Ingeniería Eléctrica, Universidad de Talca, Curicó, Chile. His main research interests include modeling and emulator design for fuel cells, design and digital control of switched converters, and energy management of hybrid electric vehicles. He is director of the Laboratory of Applications in Smart Grids (LARI in spanish) research group.

Germain Garcia received the Diploma Degree in Engineering in 1984, and the Ph-D Degree in Automatic Control in 1988, from the Institut National des Sciences Appliquèes of Toulouse, (INSAT), France. He also received the Habilitation à Diriger des Recherches (HDR) in 1997, from the University Paul Sabatier (UPS), France. He is currently researcher at the LAAS-CNRS and full professor at INSAT. His research interests include robust control theory, linear matrix inequalities (LMI), constrained control, singularly perturbed models, nonlinear control and control of power converters.

Freddy Flores-Bahamonde was born in Osorno, Chile in 1983. He received the M.Sc. and Ph.D degrees in electronics engineering from Universitat Rovira I Virgili (URV), Tarragona, Spain, in 2009 and 2013, respectively. In 2015 he joined to the Advanced center for electrical and electronic engineering (AC3E), from the Universidad Técnica Federico Santa María (UTFSM), Valparaíso, Chile, as a postdoctoral fellow. Consequently, in 2017 he was in charge of the energy area in the technology transfer unit of the AC3E developing and managing industrial projects related to the energy and electric power systems field. Dr. Flores-Bahamonde is currently Assistant Professor in the Engineering Sciences Department at the Universidad Andrés Bello, where he is also researcher in the Energy Tranformation Center. His main interest includes the design and control of power converters for renewable energies, automotive power systems, and DC microgrdis

Duberney Murillo-Yarce received the bachelor's and master's degrees in Electrical Engineering from Universidad Tecnológica de Pereira, Pereira, Colombia, in 2004 and 2010 respectively. From 2006 to 2018, he was a professor of the Faculty of Engineering at the Universidad Tecnológica de Pereira, in electric and electronic programs. Actually, he is a PhD student of Doctorate in Engineering Systems in Universidad de Talca. In addition, he is a researcher of the Laboratory of Applications, Smart Grids Research Group (LARI in Spanish). His research interests include power electronic converters, renewable energies and predictive control.

Johan I. Guzman (S'04–M'09) was born in Chile in 1976. He received his Electronic Engineering Title, his M.Sc. and D.Sc. degrees in electrical engineering from the University of Concepción in 2000, 2007 and 2009 respectively. Currently he is an associated professor at the University of Bío-Bío. His active research topics are power converters control for magnetically coupled converters, pulsed power sources for cold plasma generation and integration of ERNC in microgrids.

Marco Rivera (S'09-M'11-SM'17) received his B.Sc. in Electronics Engineering and M.Sc. in Electrical Engineering from the Universidad de Concepción, Chile in 2007 and 2008, respectively. He earned his PhD degree at the Department of Electronics Engineering, Universidad Técnica Federico Santa María, in Valparaíso, Chile, in 2011 with a scholarship from the Chilean Research Fund CONICYT. During 2011 and 2012, he was working as a postdoc researcher and part-time professor at the Department of Electronics Engineering, Universidad Técnica Federico Santa María, in Valparaíso, Chile. His research interests include matrix converters, predictive and digital controls for high-power drives, four-leg converters, and the development of high performance control platforms based on Field-Programmable Gate Arrays. Currently, he is a professor in the Department of Electrical Engineering at Universidad de Talca, Curicó, Chile. In 2013 Prof. Rivera was awarded with the Premio Tesis de Doctorado Academia Chilena de Ciencias 2012, which was awarded to the best PhD Thesis developed in 2011 for national and foreign students in any exact or natural sciences program that is a member of the Academia Chilena de Ciencias, Chile. In 2015 he was awarded as the Oustanding Engineer of 2015, award given by the Chilean Association of Electrical and Electronics Industry and the IEEE-Chile.